American Mineralogist, Volume 91, pages 475–478, 2006

LETTER

Equation of state of $CaIrO_3$-type $MgSiO_3$ up to 144 GPa

SHIGEAKI ONO,[1,*] TAKUMI KIKEGAWA,[2] AND YASUO OHISHI[3]

[1]Institute for Research on Earth Evolution, Japan Agency for Marine-Earth Science and Technology, 2-15 Natsushima-cho, Yokosuka-shi, Kanagawa 237-0061, Japan
[2]High Energy Acceleration Research Organization, 1-1 Oho, Tsukuba 305-0801, Japan
[3]Japan Synchrotron Radiation Research Institute, Mikazuki-cho, Sayo-gun, Hyogo 679-5198, Japan

ABSTRACT

The structure and equation of state for $CaIrO_3$-type $MgSiO_3$ were determined using high-pressure powder X-ray diffraction from 116 to 144 GPa. The $CaIrO_3$-type phase remained stable over this entire pressure range. At each pressure increment, the sample was heated with a laser to relax the deviatoric stress in the sample. Pressure-volume data could be fitted to the Birch-Murnaghan equation of state with K_0 = 237(1) GPa using Anderson's gold pressure standard, when K_0' and V_0 were set to 4 and 162.86 Å^3, respectively. This indicates that the bulk modulus of $MgSiO_3$ decreases when the phase transition occurs, because the bulk modulus of perovskite-type $MgSiO_3$ is 250–260 GPa. The *b* axis of the unit-cell parameter was more compressive than the *a* and *c* axes. The unit-cell volumes at high pressures, observed in high-pressure experiments, were slightly smaller than those predicted by theoretical studies.

Keywords: Post-perovskite, crystal structure, $CaIrO_3$-type structure, diamond anvil cell, $MgSiO_3$

INTRODUCTION

Recent seismological discoveries have indicated that the core-mantle boundary is likely to have more complex features than the simple boundary between the silicate mantle and liquid iron. There is an abrupt reduction in seismic wave velocity at the bottom of the lower mantle, which is called the "ultralow-velocity zone" (Mori and Helmberger 1995; Reasoner and Revenaugh 2000; Rost and Revenaugh 2003; Thorne and Garnero 2004). Some candidate explanations of this ultralow-velocity zone have been proposed. Partial melting of the mantle rock (Vidale and Hedlin 1998), chemical reactions between core and mantle materials (Song and Ahrens 1994), or underside sedimentation from the core (Buffett et al. 2000) seem to be plausible. Recently, several new models explaining the features of the ultralow-velocity zone have been proposed. (1) An iron-rich $CaIrO_3$-type (post-perovskite) phase layer exists at the bottom of the D" layer (Mao et al. 2004). (2) Subducted relics of banded iron formations have accumulated above the core (Dobson and Brodholt 2005). (3) A reversed phase transition from a $CaIrO_3$-type phase to a perovskite phase occurs at the top of the ultralow-velocity zone (Hernlund et al. 2005; Ono and Oganov 2005). The thermoelastic properties of the deep mantle minerals are key parameters for resolving the origin of the ultralow-velocity zone. Recently, the discovery of $CaIrO_3$-type $MgSiO_3$ was prompted by the observation of $CaIrO_3$-type Fe_2O_3 (Ono et al. 2004), which transforms from corundum to the Rh_2O_3-type or perovskite phase and then to the $CaIrO_3$-type phase under increasing pressure. The transition pressures from perovskite to the $CaIrO_3$-type phase in pure $MgSiO_3$ and in material equivalent in composition to pyrolite mantle have been determined by both theoretical and experimental studies (Oganov and Ono 2004; Tsuchiya et al. 2004; Ono and Oganov 2005). Theoretical studies have also determined the thermoelastic parameters of the $CaIrO_3$-type phase. Although the thermoelastic parameters are important in assessing these new models of the ultralow-velocity zone, these parameters have not been determined in high-pressure experiments.

In this study, we used laser heating and powder X-ray diffraction methods with a synchrotron radiation source. The isothermal bulk modulus of $CaIrO_3$-type $MgSiO_3$ was determined at room temperature using pressure-volume data up to 144 GPa. We also compare the structural properties predicted theoretically by ab initio calculations with those observed in this study.

EXPERIMENTAL METHODS

High-pressure X-ray diffraction experiments were performed using a laser-heated symmetrical-type diamond anvil cell (DAC) with a 50° conical aperture combined with synchrotron radiation. Synthetic $MgSiO_3$ enstatite was mechanically ground in an agate mortar to ensure homogeneity and a sufficiently fine grain size (less than a few micrometers). Gold powder, mixed with the sample, was used as an internal pressure calibrant and a heat source for laser heating. NaCl was used as a pressure-transmitting medium to reduce deviatoric stress and temperature gradients in the sample. A small pellet of the sample, with a thickness of about 10 μm, was produced using a hand press. The sample was embedded in the NaCl pressure-transmitting medium. The sample was heated with a multi-mode YAG laser to synthesize the $CaIrO_3$-type phase. The size of the heating spot was about 50 μm. After each change in pressure, the sample was heated using the YAG laser to reduce the generation of pressure inhomogeneity in the sample. After laser heating, the shape of each peak in the diffraction pattern became significantly sharper. This indicates that heating reduced the deviatoric stress in the sample chamber. Some reliable studies of equations of state for high-pressure minerals have been reported using this laser-heated annealing method (Shim et al. 2000; Andrault et al. 2003). The samples were probed with an angle-dispersive diffraction technique using a monochromatic incident X-ray beam at the synchrotron beam lines BL13A, Photon Factory (Ono et al. 2005a) and BL10XU, SPring-8 (Ono et al. 2005b).

* E-mail: sono@jamstec.go.jp

0003-004X/06/0203–475$05.00/DOI: 10.2138/am.2006.2118

The X-ray beams were collimated to a diameter of 15–30 μm, and the angle-dispersive diffraction patterns were obtained on an imaging plate. The maximum 2θ (θ = Bragg angle) value was about 25°. The incident X-ray wavelength (λ = 0.4268 or 0.4112 Å) and detector-to-sample distance (D = 290.75 or 345.96 mm) were calibrated using two X-ray diffraction patterns of a standard CeO_2 reference sample at different detector-to-sample distances. To adjust the sample position in the X-ray beam accurately, we monitored the X-ray beam intensity distribution transmitted through the DAC by scanning the DAC stage (Ono and Ohishi 2005). The scanning step was 4 μm for an area of 100 × 100 μm. Therefore, the X-ray beam position could be controlled with a precision less than 5 μm. The experimental geometry has been reported elsewhere (Ono et al. 2005a, 2005b). The observed intensities on the imaging plates were integrated as a function of 2θ using the ESRF Fit2d code (Hammersley et al. 1996). Diffraction peak positions were determined using a peak-fitting program. The pressure was determined from the observed unit-cell volume of gold from the gold equations of state of Anderson et al. (1989), Jamieson et al. (1982), and Dewaele et al. (2004). Equation of state parameters for $CaIrO_3$-type $MgSiO_3$ were obtained by a weighted least-squares fit (Angel 2000) to the pressure-volume data of the Birch-Murnaghan equation of state (Birch 1947). Rietveld refinements were also made to selected X-ray diffraction patterns using the GSAS program (Larson and von Dreele 1994). In the first step, only the scale factor and background parameters were refined. The cell constants and FWHM parameters were then refined. Finally, other parameters including the atomic coordinates were refined.

RESULTS AND DISCUSSION

At first, the sample was compressed directly at pressures higher than 120 GPa, corresponding to the stability field of $CaIrO_3$-type $MgSiO_3$, which was determined by both theoretical and experimental studies (Oganov and Ono 2004; Tsuchiya et al. 2004; Ono and Oganov 2005). Before laser heating, the diffraction pattern showed broad peaks for gold and B2-type NaCl and no $MgSiO_3$ phases were synthesized. Next, the sample was heated to about 1500–2500 K to relax the differential stress and to synthesize $CaIrO_3$-type $MgSiO_3$. After confirmation that many new peaks appeared during heating in addition to the diffraction peaks for gold and NaCl, the temperature was reduced slowly to 300 K, because rapid temperature quenching induces a significant differential stress in the sample chamber. The powder X-ray diffraction data for the sample at 300 K revealed that the synthesized $MgSiO_3$ phase had a $CaIrO_3$-type structure with an orthorhombic cell (space group, *Cmcm*). Figure 1 shows the Rietveld refinement for a selected pattern of the $CaIrO_3$-type structure of $MgSiO_3$ after laser heating. The determined atomic coordination is shown in Table 1. In $CaIrO_3$-type $MgSiO_3$, Z = 2, with sixfold silicon and eightfold magnesium coordinations. The SiO_6 octahedra share edges and the octahedral sheets are stacked along the *b* axis with an interlayer of magnesium atoms. Table 1 also shows a comparison of the observed and predicted cell parameters and atomic coordinations. The observed data in this study are generally consistent with those predicted by ab initio calculations (Oganov and Ono 2004; Tsuchiya et al. 2004).

The sample was heated with the laser after each pressure increment, before the X-ray diffraction measurements were made. In addition to the diffraction peaks for $CaIrO_3$-type $MgSiO_3$, there were some intense diffraction peaks for both the internal pressure calibrant, gold, and the pressure-transmitting medium, NaCl. However, most diffraction lines that were free from interference allowed $CaIrO_3$-type $MgSiO_3$ to be identified and its unit-cell dimensions to be refined. The measured unit-cell parameters and volumes are shown in Table 2. The *b* axis was approximately 30% more compressible than the *a* or *c* axis, which had similar compressibilities.

The variation in the volume of $CaIrO_3$-type $MgSiO_3$ with pressure is shown in Figure 2. The pressure-volume data were used for a least-squares fit of the Birch-Murnaghan equation of state,

$$P = \frac{3}{2}K_0(x^{-7} - x^{-5})[1 + \frac{3}{4}(K_0' - 4)(x^{-2} - 1)]$$

where $x = (\frac{V}{V_0})^{\frac{1}{3}}$; and V_0, K_0, and K_0' are the volume, the isothermal bulk modulus, and the first pressure derivative of the isothermal bulk modulus, respectively. Because $CaIrO_3$-type $MgSiO_3$ could not be quenched to ambient pressure, the uncertainties of V_0 and

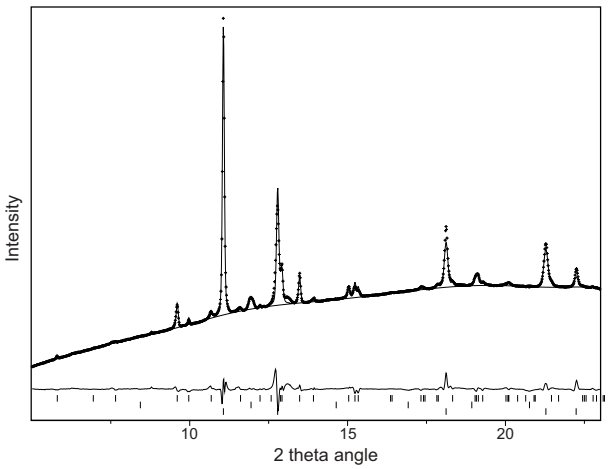

FIGURE 1. Rietveld refinement for $CaIrO_3$-type $MgSiO_3$. The raw data (crosses) were obtained at 116 GPa and 300 K (after heating). The upper and lower solid lines represent the calculated and the difference curves, respectively. The wavelength of the monochromatic incident X-ray beam was 0.4112 Å. The vertical bars show the reflection positions for each phase (upper, $CaIrO_3$-type $MgSiO_3$; middle, B2-type NaCl; lower, gold). The refined structural parameters are shown in Table 1.

TABLE 1. Comparison of structural data for the $CaIrO_3$-type $MgSiO_3$

		Experiment	Theory*	Theory†
Cell parameters				
	a (Å)	2.4687(5)	2.4738	2.462
	b (Å)	8.1165(20)	8.1209	8.053
	c (Å)	6.1514(13)	6.1382	6.108
	V (Å³)	123.26(3)	123.31	121.10
Atomic coordinates				
Mg (0,*y*,1/4)	*y*	0.2565(16)	0.2532	0.253
Si (0,0,0)				
O1 (0,*y*,1/4)	*y*	0.9430(26)	0.9276	0.927
O2 (0,*y*,*z*)	*y*	0.6400(14)	0.6356	0.637
	z	0.4424(25)	0.4413	0.441
Interatomic distances				
	Mg-O1 (Å)	1.953 (×2)	1.880 (×2)	1.865 (×2)
	Mg-O2 (Å)	1.954 (×4)	1.955 (×4)	1.936 (×4)
		2.070 (×2)	2.099 (×2)	2.084 (×2)
	Si-O1 (Å)	1.606 (×2)	1.643 (×2)	1.636 (×2)
	Si-O2 (Å)	1.715 (×4)	1.695 (×4)	1.692 (×4)

Notes: Experimental data were obtained at 116 GPa and 300 K.
* Oganov and Ono (2004) at 120 GPa.
† Tsuchiya et al. (2004) at 120 GPa. Space group of $CaIrO_3$-type phase is *Cmcm* (Z = 4). Reliability factors are $R_p = 0.0074$, $R_{wp} = 0.0152$, $R_f^2 = 0.1567$, and $D_{dw} = 0.186$. $R_p = [\Sigma|I_{obs}-I_{cal}|]/\Sigma I_{obs}$. $R_{wp} = \{\Sigma[w(I_{obs}-I_{cal})^2]/\Sigma[wI_{obs}^2]\}^{1/2}$, where I_{obs} = observed intensity, I_{cal} = calculated intensity, and $w = 1/I_{obs}$. $R_f^2 = R$-structure factor based on observed and calculated structure amplitudes. D_{dw} = Durbin-Watson index.

TABLE 2. Lattice parameters and volumes of $CaIrO_3$-type $MgSiO_3$ to 144 GPa

Gold				$MgSiO_3$			
a (Å)	P (GPa)*	P (GPa)†	P (GPa)‡	a (Å)	b (Å)	c (Å)	V (Å^3)
3.6862 (2)	116.1(1)	111.5(1)	121.4(1)	2.469 (1)	8.117 (3)	6.151 (2)	123.26 (8)
3.6654 (5)	128.5(3)	122.7(3)	134.4(3)	2.462 (3)	8.070 (8)	6.090 (7)	121.01 (23)
3.6572 (9)	133.6(5)	127.3(5)	139.7(5)	2.250 (3)	8.026 (7)	6.107 (7)	120.11 (22)
3.6480 (5)	139.5(3)	132.6(3)	145.9(3)	2.444 (4)	8.029 (9)	6.073 (7)	119.17 (26)
3.6455 (8)	141.2(5)	134.1(5)	147.7(5)	2.439 (2)	7.990 (6)	6.072 (4)	118.33 (16)
3.6407 (5)	144.4(2)	137.0(2)	151.1(2)	2.436 (3)	7.986 (7)	6.061 (5)	117.91 (19)

Notes: Numbers in parentheses represent the error of lattice parameters.
* Anderson et al. (1989).
† Jamieson et al. (1982).
‡ Dewaele et al. (2004).

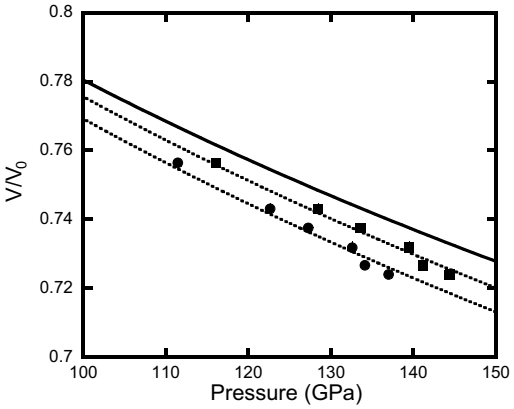

FIGURE 2. Pressure-volume data for $CaIrO_3$-type $MgSiO_3$ at 300 K. The powder X-ray diffraction results are shown by the squares (Anderson et al. 1989) and circles (Jamieson et al. 1982). Dashed curves: third-order Birch-Murnaghan equation fit, K_0 = 236(1) and 225(1) GPa, K_0' is fixed to 4, using Anderson's and Jamieson's pressure scales. V_0 is fixed to 162.86 Å^3, which was obtained with a theoretical study using the local density approximation (LDA) method (Oganov and Ono 2004). The solid line represents the volume change of $CaIrO_3$-type $MgSiO_3$ calculated by Oganov and Ono (2004).

K_0' are likely to be large. Therefore, the data were constrained by fixing K_0' equal to 4. V_0 was also fixed to 162.86 Å^3, which was calculated theoretically (Oganov and Ono 2004). The error in pressure was less than 0.5 GPa, based on the lattice parameters calculated from the gold diffraction lines. However, using different equation of state values for the gold pressure calibrant, the discrepancy in experimental pressure was greater than 10 GPa at very high pressures (Jamieson et al. 1982; Anderson et al. 1989; Dewaele et al. 2004). Therefore, we estimated the equation of state for $CaIrO_3$-type $MgSiO_3$ using each equation of state determined for the gold pressure calibrant. Using all the data, values of 237(1), 226(1), and 248(1) GPa were obtained for Anderson's, Jamieson's, and Dewaele's gold standards, respectively. The volume data predicted by theoretical calculations are also plotted in Figure 2. The predicted volumes of $CaIrO_3$-type $MgSiO_3$ were slightly greater than those obtained in our experiments.

It was difficult to acquire volume data for $CaIrO_3$-type $MgSiO_3$ at pressures below 110 GPa, because the $CaIrO_3$-type structure is metastable under these conditions. There seems to be significant uncertainty in the estimated parameters of the equation of state at 0 GPa. Therefore, we also calculated the isothermal bulk modulus and volume using Anderson's gold standard (Anderson et al. 1989) at 110 GPa, which corresponds to the transition pressure of $CaIrO_3$-type $MgSiO_3$. Refinement yielded the equation-of-state parameters K_{110GPa} = 577(20) GPa and V_{110GPa} = 124.50(13) Å^3 when the first pressure derivative of the bulk modulus was fixed at 4.

TABLE 3. Comparison of the isothermal bulk modulus of $CaIrO_3$- and perovskite-type $MgSiO_3$

K_0 (GPa)	K_0'	V_0 (Å^3)	P standard	References
		$CaIrO_3$-type		
237(1)	4 (fixed)	162.86(fixed)	Au*	This study
226(1)	4 (fixed)	162.86(fixed)	Au†	This study
248(1)	4 (fixed)	162.86(fixed)	Au‡	This study
231.93	4.43	162.86		LDA calculation§
222	4.2	163.81		LDA calculation‖
		Perovskite-type		
261	4 (fixed)	162.49	Au*	Mao et al. (1991)
253	3.9	162.27	Pt††	Fiquet et al. (2000)

Notes: K_0 and K_0' are the isothermal bulk modulus and the first derivative of the isothermal bulk modulus at 300 K. Different pressure scales were used to calculate the isothermal bulk modulus.
* Anderson et al. (1989).
† Jamieson et al. (1982).
‡ Dewaele et al. (2004).
§ Oganov and Ono (2004).
‖ Tsuchiya et al. (2004).

The isothermal bulk modulus determined in this study is compared with those from other studies in Table 3. The room-temperature bulk modulus determined in this study is in excellent agreement with those at 0 K predicted by ab initio calculations (Oganov and Ono 2004; Tsuchiya et al. 2004). In general, the bulk modulus increases when the pressure-induced phase transformation occurs, because the dense structure is less compressible at high pressures. However, previous theoretical studies have predicted that the bulk modulus of $MgSiO_3$ decreases when the perovskite-$CaIrO_3$ transition occurs. The bulk moduli of perovskite-type $MgSiO_3$ determined in previous experimental studies are also shown in Table 3. The bulk modulus of $CaIrO_3$-type $MgSiO_3$ determined in this study is smaller than those of perovskite-type $MgSiO_3$. This indicates that the values measured in high-pressure experiments are consistent with theoretical predictions.

ACKNOWLEDGMENTS

We are grateful to A.R. Oganov for fruitful discussions. The synchrotron radiation experiments were performed at the PF, KEK (Proposal No. 2003G187) and at the SPring-8, JASRI (proposal no. 2003A0013-LD2-np). This work was partially supported by the Ministry of Education, Culture, Sport, Science and Technology, Japan.

REFERENCES CITED

Anderson, O.L., Isaak, D.G., and Yamamoto, S. (1989) Anharmonicity and the equation of state for gold. Journal of Applied Physics, 65, 1534–1543.

Andrault, D., Angel, R.J., Mosenfelder, J.L., and Le Bihan, T. (2003) Equation of state of stishovite to lower mantle pressures. American Mineralogist, 88, 301–307.

Angel, R.J. (2000) Equations of state, In R.M. Hazan and R.T. Downs, Eds., High-pressure, high-temperature crystal chemistry, 41, p. 35–60. Reviews in Mineralogy and Geochemistry, Mineralogical Society of America, Chantilly, Virginia.

Birch, F. (1947) Finite elastic strain of cubic crystals. Physical Review, 71, 709–824.

Buffett, B.A., Garnero, E.J., and Jeanloz, R. (2000) Sediments at the top of Earth's core. Science, 290, 1338–1342.

Dewaele, A., Loubeyre, P., and Mezouar, M. (2004) Equations of state of six metals above 94 GPa. Physical Review B, 70, 094112.

Dobson, D.P. and Brodholt, J.P. (2005) Subducted banded iron formations as a source of ultralow-velocity zones at the core-mantle boundary. Nature, 434, 371–374.

Fiquet, G., Dewaele, A., Andrault, D., Kunz, M., and Le Bihan, T. (2000) Thermoelastic properties and crystal structure of $MgSiO_3$ perovskite at lower mantle pressure and temperature conditions. Geophysical Research Letters, 27, 21–24.

Hammersley, A.P., Svensson, S.O., Hanfland, M., Fitch, A.N., and Häusermann, D. (1996) Two-dimensional detector software: From real detector to idealized image or two-theta scan. High Pressure Research, 14, 235–245.

Hernlund, J.W., Thomas, C., and Tackley, P.J. (2005) A doubling of the post-perovskite phase boundary and structure of the Earth's lowermost mantle. Nature, 434, 882–886.

Jamieson, J.C., Fritz, J.N., and Manghnani, M.H. (1982) Pressure measurement at high temperature in X-ray diffraction studies: gold as a primary standard. In S. Akimoto and M.H. Manghnani, Eds., High-Pressure Research in Geophysics, p. 27–48. Center for Academic Publishing, Tokyo.

Larson, A.C. and von Dreele, R.B. (1994) General Structure Analysis System, Los Alamos Laboratory, Report No. LAUR 85-758.

Mao, H.K., Hemley, R.J., Fei, Y., Shu, J.F., Chen, L.C., Jephcoat, A.P., Wu, Y., and Basset, W.A. (1991) Effect of pressure, temperature and composition on the lattice parameters and density of three $(Fe,Mg)SiO_3$ perovskite up to 30 GPa. Journal of Geophysical Research, 101, B8257–B8269.

Mao, W.L., Shen, G., Prakapenka, V.B., Meng, Y. Campbell, A.J., Heinz, D.L., Shu, J., Hemley, R.J., and Mao, H-K. (2004) Ferromagnesian postperovskite silicates in the D" layer of the Earth. Proceedings of the National Academy of Sciences of the United States of America, 101, 15867–15869.

Mori, J. and Helmberger, D.V. (1995) Localized boundary layer below the mid-Pacific velocity anomaly from a PcP precursor. Journal of Geophysical Research, 100, 20359–20365.

Oganov, A.R. and Ono, S. (2004) Theoretical and experimental evidence for a post-perovskite phase of $MgSiO_3$ in Earth's D" layer. Nature, 430, 445–448.

Ono, S. and Oganov, A.R. (2005) In situ observations of phase transition between perovskite and $CaIrO_3$-type phase in $MgSiO_3$ and pyrolitic mantle composition. Earth and Planetary Science Letters, 236, 914–932.

Ono, S. and Ohishi, Y. (2005) In situ X-ray observation of phase transformation in Fe_2O_3 at high pressures and high temperatures. Journal of Physics and Chemistry of Solids, 66, 1714–1720.

Ono, S., Kikegawa, T., and Ohishi, Y. (2004) High-pressure phase transition of hematite, Fe_2O_3. Journal of Physics and Chemistry of Solid, 65, 1527–1530.

Ono, S., Funakoshi, K., Nozawa, A., and Kikegawa, T. (2005a) High-pressure phase transitions in SnO_2. Journal of Applied Physics, 97, 073523.

Ono, S., Funakoshi, K., Ohishi, Y., and Takahashi, E. (2005b) In situ X-ray observation of phase transition between hematite-perovskite structures in Fe_2O_3. Journal of Physics. Condensed Matter, 17, 269–276.

Reasoner, C. and Revenaugh, J. (2000) ScP constraints on ultralow-velocity zone density and gradient thickness beneath the Pacific. Journal of Geophysical Research, 105, 28173–28182.

Rost, S. and Revenaugh, J. (2003) Small-scale ultralow-velocity zone structure imaged by ScP. Journal of Geophysical Research, 108, 2056.

Shim, S.H., Duffy, T.S., and Shen, G. (2000) The equation of state of $CaSiO_3$ perovskite to 108 GPa at 300 K. Physics and Chemistry of Minerals, 120, 327–338.

Song, X. and Ahrens, T.J. (1994) Pressure-temperature range of reactions between liquid iron in the outer core and mantle silicates. Geophysical Research Letters, 21, 153–156.

Thorne, M. and Garnero, E.J. (2004) Interferences on ultralow-velocity zone structure from a global analysis of SPdKS waves. Journal of Geophysical Research, 109, B08301.

Tsuchiya, T., Tsuchiya, J., Umemoto, K., and Wentzcovitch, R.M. (2004) Phase transition in $MgSiO_3$ perovskite in the Earth's lower mantle. Earth and Planetary Science Letters, 224, 241–248.

Vidale, J.E. and Hedlin, M.A.H. (1998) Evidence for partial melt at the core-mantle boundary north of Tonga from the strong scattering of seismic waves. Nature, 391, 682–685.

MANUSCRIPT RECEIVED OCTOBER 11, 2005
MANUSCRIPT ACCEPTED NOVEMBER 21, 2005
MANUSCRIPT HANDLED BY BRYAN CHAKOUMAKOS